Journal of Theoretical Biology 364 (2015) 397–406

Contents lists available at ScienceDirect

Journal of Theoretical Biology

journal homepage: www.elsevier.com/locate/yjtbi

Determining equilibrium osmolarity in poly(ethylene glycol)/chondrotin sulfate gels mimicking articular cartilage

S. Sircar [a,*], E. Aisenbrey [b], S.J. Bryant [b,c,d], D.M. Bortz [e]

[a] School of Mathematical Sciences, University of Adelaide, SA 5000, Australia
[b] Department of Chemical & Biological Engg., University of Colorado, Boulder, CO 80309, United States
[c] BioFrontiers Institute, University of Colorado, Boulder, CO 80309, United States
[d] Material Science and Engineering Program, University of Colorado, Boulder, CO 80309, United States
[e] Department of Applied Mathematics, University of Colorado, Boulder, CO 80309-0526, USA

HIGHLIGHTS

- A comprehensive model of a multi-phase, multi-species polyelectrolyte gel model is proposed.
- Model features include: elasticity via covalent cross-links in the polymer network, microscopic nearest-neighbor interaction between the various polymer/solvent species, electrostatic and osmotic pressure.
- *In vivo* studies are conducted and the equilibrium electrochemical composition are compared with the model output.
- It is generally seen that swelling is aided in the case of a highly charged gel with low cross-link fractions or the ones immersed in a bath with low solute concentration or a high pH.
- A de-swelled state of the gel is preferred at high cross-link fraction and higher average charge per monomer.

ARTICLE INFO

Article history:
Received 15 August 2013
Received in revised form
15 September 2014
Accepted 27 September 2014
Available online 7 October 2014

Keywords:
Polyelectrolyte gel
Multi-phase mixture
Donnan potential
Cross-links
Hydrogel

ABSTRACT

We present an experimentally guided, multi-phase, multi-species polyelectrolyte gel model to make qualitative predictions on the equilibrium electro-chemical properties of articular cartilage. The mixture theory consists of two different types of polymers: poly(ethylene gylcol) (PEG), chondrotin sulfate (ChS), water (acting as solvent) and several different ions: H^+, Na^+, Cl^-. The polymer chains have covalent cross-links whose effect on the swelling kinetics is modeled via Doi rubber elasticity theory. Numerical studies on equilibrium polymer volume fraction and net osmolarity (difference in the solute concentration across the gel) show a complex interplay between ionic bath concentrations, pH, cross-link fraction and the average charge per monomer. Generally speaking, swelling is aided due to a higher average charge per monomer (or a higher particle fraction of ChS, the charged component of the polymer), low solute concentration in the bath, a high pH or a low cross-link fraction. A peculiar case arises at higher values of cross-link fraction, where it is observed that increasing the average charge per monomer leads to gel deswelling.

1. Introduction

Articular cartilage is a polyelectrolyte biogel that forms a thin tissue layer lining the articulating ends of all diarthrodial joints in the body and contribute to the lubrication mechanisms in the joint (Mow and Ratcliffe, 1997). The water phase of cartilage constitutes on average from 60 to 80% of the total weight for normal tissue while the dominant structural components of the solid matrix are the collagen molecules and proteoglycans (PGs) (Mow et al., 1993). The collagen fibrils are densely packed polymer strands with a high resistance against fluid flow (Armstrong and Mow, 1982), which helps in retaining the shape of the cartilage when compressed (Maroudas, 1979). PGs are macromolecules consisting of a protein core to which are attached short chains of negatively charged glycosaminoglycans (GAGs) (Setton et al., 1993). The primary GAGs associated with PGs in cartilage are chondroitin 4-sulfate, chondroitin 6-sulfate and keratan sulfate (Maroudas, 1979).

An increase in cartilage tissue hydration, governed by the density and the nature of fixed charges on the PGs as well as the density of the mobile counter ions in the interstitial fluid are the earliest signs of articular cartilage degeneration during

* Corresponding author.
E-mail address: sarthok.sircar@adelaide.edu.au (S. Sircar).

http://dx.doi.org/10.1016/j.jtbi.2014.09.037
0022-5193/

osteoarthritis (Armstrong and Mow, 1982; Maroudas, 1979). For this reason the development of mathematical models and numerical methods to quantify cartilage swelling have been of great interest for many years. Each PG-associated negative charge on the polymer chain (known as the fixed charge), requires a mobile counter-ion (e.g., Na^+) dissolved within the interstitial fluid in the cartilage gel to maintain its electro-neutrality (Maroudas et al., 1991). This effect gives rise to an imbalance of mobile ions across the gel interface. The excess of mobile ions colligatively yields a swelling pressure, known as the osmotic pressure (Maroudas, 1968), while the swelling pressure associated with the fixed charges is known as the Donnan pressure (Donnan, 1924). Changes in this internal swelling pressure, arising from altered ion concentrations of the external bath, or changes in the fixed charges result in changes in tissue dimensions and hydration. However, this swelling pressure is balanced by tensile forces generated in the collagen network (Muir et al., 1970). This effect is due to the presence of covalent cross-links within the gel matrix.

Mathematical models are essential for understanding systems with many interacting components (e.g. the collagen network, proteoglycans, interstitial fluid and ionic solutions present in cartilage), since the complexity of the interactions taking place overwhelms the ability of the human intuition to make accurate predictions of their behavior. Early work in this direction began with the classical work of Flory (1953), Flory and Rehner (1943a, 1943b) and Katchalsky and Michaeli (1955) (see also Doi and Edwards, 1986; Flory, 1976) to understand the swelling and deswelling of hydrogels. In this theory, the free energy is used to make predictions about the thermodynamical equilibrium configurations of polymer gels and their dependence on environmental parameters such as temperature or solvent ion concentrations. An important problem is to understand how the kinetics (and not simply the equilibria) of swelling and deswelling is governed. An early answer was given by Tanaka and Filmore (1979) and Tanaka et al. (1980) who developed a kinetic theory of swelling gels viewing a gel as a linear elastic solid immersed in a viscous fluid. Subsequent studies relaxed the assumption of linear elasticity by defining the force on the gel to be the functional derivative of the free energy function for the polymer mesh (Durning and Morman, 1993; Maskawa et al., 1999; Onuki, 1989; Sekimoto et al., 1989; Yamaue et al., 2000). However, most of these works neglected the fluid flow that must accompany swelling. Wang et al. (1997) added fluid flow by application of two-phase flow theory but considered only small polymer volume fractions and small gradients in the volume fraction. Durning and Morman (1993) also used continuity equations to describe the flow of solvent and solution in the gel, but used a diffusion approximation with a constant diffusion coefficient to determine the fluid motion. Similarly, mathematical models and simulations of polyelectrolyte gels have been developed by other groups, in an effort to examine the effect of fixed charge density via Donnan potential (English et al., 1996; Wolgemuth et al., 2004; Hou et al., 1989; Lai et al., 1991; Gu et al., 1998), Nernst-Planck motion of ions (Setton et al., 1993; Dhanarajan et al., 2002) and van't Hoff osmotic pressure (Lanir, 1996), in cartilage. These efforts include using the Poisson–Boltzmann equation and Biot's theory of poroelasticity (De et al., 2002), as well as phenomenological modifications of Flory–Higgins theory to capture some effects of multi-ionic cations (Kokufuta, 2005; Hirotsu, 1991; Zribi et al., 2006). However, these current state of the art models do not couple the binding/unbinding of the ions to the network micro-structure (Calderer et al., 2013). The National Institute of Health (NIH) states that these binding/unbinding events are critical to describing the local ion environment inside cartilage, the environment that cells 'see', and the bulk mechanical properties of the tissue and/or polymer (Health, United States, 2006).

In this regard, the innovative approach of this work is to create the next generation, multi-phase, mechanistic ionic gel-swelling model which mimics the equilibrium, free swelling/deswelling environment within the articular cartilage and which captures all of the fundamental scientific elements mentioned above. Using this model we will outline how to extract the information from the macro-scale data of gel-swelling (derived via in vivo experiments) and help explain some micro-scale effects (e.g., details on polymer cross-linked structure). To calibrate the outcome of this model, in vitro set-ups of cross-linked copolymerized poly(ethylene glycol) (PEG) and chondrotin sulfate (ChS) gels were developed (Bryant and Anseth, 2003; Bryant et al., 2004; Villanueva et al., 2010). PEG was chosen since it can be functionalized to enable cross-linking to form a 3-D matrix, a system that promotes the deposition of proteoglycans and collagen molecules and emulates the mechanical strength, load bearing capabilities and resilience of cartilage tissue (Bryant and Anseth, 2003). The ChS component serves two purposes: to mimic the biochemical environment of cartilage (since it is the main component of proteoglycans) and to introduce fixed negative charges into the network (Bryant et al., 2004). In the next section, we present the details of this model, including the chemical potentials (Section 2.1) and the chemistry of the binding reaction at quasi-equilibrium conditions (Section 2.2). Further, we provide the details of the in vitro gel-swelling experiments (Section 3) and the methods to estimate the model parameters (Section 4). The results pertaining to the equilibrium configuration of these ionic gels under different electro-chemical stimuli are presented in Section 5. We conclude with a brief discussion of the implication of these results and the focus of our future directions.

2. Multi-species, multi-phase cartilage-gel model

We view the PEG-gel with negatively charged ChS strands in ionic solution, as a multi-component material, including solvent particles, polymer and particles of several ionic species. The polymer is assumed to be made up of two types of monomers the uncharged units (PEG segment of the polymer) and those that are the charged ones (ChS segment of the polymer). Only the charged units participate in the binding reactions, carry a double negative charge and are denoted as M^{2-}. The positively charged ions in the solvent are Hydrogen (H^+) and Sodium (Na^+). The negatively charged ions could include Hydronium (OH^-) and Chloride (Cl^-). Because the negatively charged ions are assumed to be not involved in any binding reactions with the gel, acting only as counterions to positive charges, we identify these ions by the name Chloride. The binding reactions of the positively charged ions with the monomers are

$$
\begin{aligned}
&(a)\ M^{2-} + H^+ \underset{k_{-h}}{\overset{k_h}{\rightleftharpoons}} MH^-,\\
&(b)\ M^{2-} + Na^+ \underset{k_{-n}}{\overset{k_n}{\rightleftharpoons}} MNa^-,\\
&(c)\ MH^- + H^+ \underset{k_{-h2}}{\overset{k_{h2}}{\rightleftharpoons}} MH_2,\\
&(d)\ MNa^- + Na^+ \underset{k_{-n2}}{\overset{k_{n2}}{\rightleftharpoons}} MNa_2,\\
&(e)\ MH^- + Na^+ \underset{k_{-hn}}{\overset{k_{hn}}{\rightleftharpoons}} MHNa.
\end{aligned}
\tag{1}
$$

We assume that all the binding sites/charge sites are identical and the binding affinities for the different ions are different. The species M^{2-}, MH^-, MNa^-, MH_2, MNa_2 and MHNa are different monomer species of the charged type, all of which move with the same polymer velocity. The ion species are freely diffusible, but because they are ions, their movement is restricted by the requirement to maintain electroneutrality. Finally, because a small amount of water dissociates into hydrogen and hydronium, we are

guaranteed that there are always some positive and negative ions in the solvent.

Suppose we have some volume V of a mixture comprised of k types of particles each with particle density (number of particles per unit volume) n_j, and particle volumes ν_j, $j=1,\ldots,k$. From now on we will denote the quantities with subscript "1" related to PEG monomer species, subscript "2" related to ChS monomer species and subscript "3" related to solvent molecule. The subscript (p,s) denotes polymer and solvent phase, respectively. The volume fraction for each of the polymer species (θ_1,θ_2) and the solvent $(\theta_3=\theta_s)$ are $\theta_i=\nu_i n_i$ $(i=1,\ 2,\ 3)$ respectively and $\theta_p=\theta_1+\theta_2$. Suppose the ChS monomers constitute a fraction 'α' of the total number of monomers, n_p, (i.e., $n_2=\alpha n_p$, $n_1=(1-\alpha)n_p$). Assuming that the ionic species do not contribute significantly to the volume (i.e., we take $\nu_j=0$, $j=4,\ldots,k$), conservation of total volume implies $\theta_1+\theta_2+\theta_3=1$. Further, in subsequent calculations we make an assumption that the particle density of the ions is insignificantly small compared to the particle density of polymer and solvent, i.e. $\sum_{j\geq 4} n_j \ll n_s+n_p$. Hence, $\phi_s=n_s/(n_p+n_s)$, $\phi_p=n_p/(n_p+n_s)$, $\phi_j=n_j/\sum_{i\neq 1,2} n_i$ for $j\geq 4$ (assuming that the ions are dissolved in the solvent), are the polymer, solvent, and ion species per total solvent particle fractions, respectively.

2.1. Chemical potential

This section outlines the calculation of the free energy and the chemical potential for this multi-species material. As above, we suppose there are k different kinds of particles, with particle volumes ν_i and particle numbers $n_i, i=1,\ldots,k$. To calculate the chemical potentials, μ_j, we use Gibb's free energy

$$G=-k_BTS+U+PV, \tag{2}$$

where U is internal energy, S is entropy, T is temperature, k_B is Boltzmann's constant, P is pressure, and $V=\sum_j \nu_j n_j$ is the total volume of the system. However, we assume that the volume occupied by species $j=4,\ldots,k$ (which are the ions dissolved in the solvent) is small compared to that of the monomer plus solvent volumes $\nu_p n_p+\nu_s n_s$ and so take $V=\nu_p n_p+\nu_s n_s$. The chemical potential is given by

$$\mu_j=\frac{\partial G}{\partial n_j}=-k_BT\frac{\partial S}{\partial n_j}+\frac{\partial U}{\partial n_j}+\nu_j P=\mu_j^S+\mu_j^I+\nu_j P, \tag{3}$$

where μ_j^S, μ_j^I are the contribution due to entropy and internal energy respectively. In the next two sections these two contributions to the chemical potential are derived.

2.1.1. Entropic contributions to chemical potentials

The entropy of the system is defined as

$$S=\sum n_i\omega_i, \tag{4}$$

where ω_i is the entropy per particle for the ith particle. Using standard counting arguments (Doi, 1996), for single-molecule species,

$$\omega_j=-\ln(\phi_j)\quad j\geq 3 \tag{5}$$

The PEG and ChS chains exhibit permanent cross-link bonds (i.e., covalent bonds), and we calculate the per-particle entropy of these two species using the rubber elasticity theory (Doi, 2009)

$$\omega_i=-\frac{3k_i}{2N_i}\left[(\phi_i)^{-2/3}-1\right],\quad i=1,2, \tag{6}$$

where $i=1,2$ corresponds to PEG and ChS polymer species respectively. The corresponding particle fractions are $\phi_1=(1-\alpha)\phi_p$ and $\phi_2=\alpha\phi_p$. k_i and N_i are the fractions representing the number of cross-linked monomers per total number of monomers in one chain, and the number of monomers per chain, respectively. Using Eq. (3), the entropic contribution to the chemical potentials for different species are

$$\frac{\mu_p^S}{k_BT}=\frac{k_1}{N_1}\phi_1^{-2/3}\left[\phi_1+\frac{1-\alpha}{2}\right]+\frac{k_2}{N_2}\phi_2^{-2/3}\left[\phi_2+\frac{\alpha}{2}\right]-\frac{3}{2}\left[\frac{k_1}{N_1}(1-\alpha)+\frac{k_2}{N_2}\alpha\right]-\phi_s, \tag{7a}$$

$$\frac{\mu_s^S}{k_BT}=\ln\phi_s+\phi_p+\frac{k_1}{N_1}\phi_1^{1/3}+\frac{k_2}{N_2}\phi_2^{1/3}-\sigma_I, \tag{7b}$$

$$\frac{\mu_j^S}{k_BT}=\ln\phi_j+1-\sigma_I,\qquad j\geq 4, \tag{7c}$$

where $\sigma_I=\sum_{i\geq 4}\phi_j$ is the total ion particle fraction and represents osmotic pressure as characterized by van't Hoff's law.

2.1.2. Internal energy contribution to chemical potentials

The internal energy consists of two contributions, long range electrostatic interactions and short range (nearest neighbor) interactions. The long range electrostatic interactions have energy

$$U_e=\sum_j z_j n_j \Phi_e, \tag{8}$$

where z_i is the charge on the ith ionic species ($z_1=z_2\equiv z_p$ is the average charge per monomer), and Φ_e is the electric potential.

To calculate the short range interaction energy for the polymer and solvent, we assume that each of the n_T $(=n_p+n_s)$ particles have z neighboring interaction sites (called the coordination number). Of the total of n_p monomers, k_1n_1 and k_2n_2 of them are the cross-linked PEG and ChS monomers, respectively. Since the cross-linked particles are pair-wise connected, we treat each of these pair as a single species.

The different species with their pairwise interactions (i.e., the cross-linked species, x, the uncross-linked species, u, and the solvent particles, s) are shown in Fig. 1. Following assumptions are made while calculating the per-particle interaction energy, U: (1) all cross-links are assumed identical, (2) the cross-links are covalent permanent bonds (unlike the case of transient cross-links, Sircar et al., 2013), (3) the polymers have long chains and hence the end-effects are neglected and (4) different polymer species have the same interaction energies if they are of the same type (e.g., uncross-linked PEG and uncross-linked ChS monomers have the same interaction energy). The cross-linked particle pair and the uncross-linked monomer have $2z$-6 and z-2 free interaction sites based on their position in the middle of the polymer chain, respectively (Fig. 1a and b). The solvent particles have z free interaction sites (Fig. 1c).

We let $k_BT_0\epsilon_{xx}$, $k_BT_0\epsilon_{uu}$, $k_BT_0\epsilon_{pp}$, $k_BT_0\epsilon_{us}$ and $k_BT_0\epsilon_{ss}$ be the interaction energies associated with the covalent cross-links, uncross-linked monomer–monomer interaction, monomer–monomer interaction within a polymer strand, monomer–solvent interaction and solvent–solvent interaction, respectively. T_0 is a reference temperature. The interaction energies for crosslinked,

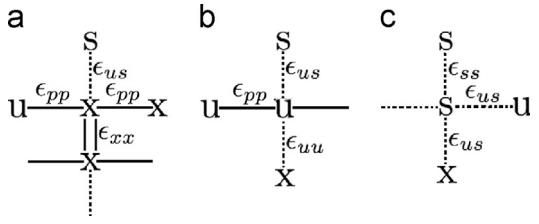

Fig. 1. Pairwise interactions of the different species and their associated interaction energies for: (a) cross-linked monomers, x, (b) uncross-linked monomers, u, and (c) solvent, s. Double solid lines denote cross-linking, single solid lines denote interactions within a polymer chain while the other types of interactions are denoted by dashed lines. The nearest neighbor interactions are assumed identical for both the PEG and ChS monomer species.

uncrosslinked polymer particles, and solvent particles are

$$\frac{F_x}{k_BT_0}=\left(\frac{n_1}{2}k_1^2+\frac{n_2}{2}k_2^2+\frac{n_1+n_2}{2}k_1k_2\right)(2\epsilon_{xx}+(2z-6)E_{us}+4\epsilon_{pp}), \tag{9a}$$

$$\frac{F_u}{k_BT_0}=((1-k_1)n_1+(1-k_2)n_2)((z-2)E_{us}+2\epsilon_{pp}), \tag{9b}$$

$$\frac{F_s}{k_BT_0}=zn_s\left(\epsilon_{us}\frac{n_m}{n_T}+\epsilon_{ss}\frac{n_s}{n_T}\right), \tag{9c}$$

respectively, where $E_{us}=\epsilon_{uu}(n_p/n_T)+\epsilon_{us}(n_s/n_T)$. Each of these is calculated using standard mean-field arguments. For example, for F_x (Fig. 1a), there are either $n_1/2$ pairs of only PEG monomers, $n_2/2$ pairs of only ChS monomers or $(n_1+n_2)/2$ pairs of both PEG and ChS monomers, respectively. The corresponding probabilities of forming cross-links are k_1^2, k_2^2 and k_1k_2. For each of these pairs, two neighboring sites are occupied by the covalent cross-link, four neighboring interactions are the monomer–monomer interactions within the polymer strands, and the remaining $z-6$ interactions are distributed to monomer–monomer, with probability n_p/n_T and monomer–solvent, with probability n_s/n_T.

Using the relations, $n_1=(1-\alpha)n_p, n_2=\alpha n_p$, it follows that the total per particle interaction energy is

$$\begin{aligned}U&=\frac{1}{2(n_m+n_s)}(F_x+F_u+F_s)\\&=k_BT_0\left[\chi\phi_p\phi_s+\mu_0^s\phi_s+\mu_0^p\phi_p+\frac{z}{2}\epsilon_{us}\right],\end{aligned} \tag{10}$$

where

$$\begin{aligned}\chi=&\frac{z}{2}\epsilon_1(k_1k_2-(1-\alpha)k_1(1-k_1)-\alpha k_2(1-k_2))\\&+\frac{z}{2}\epsilon_2+\epsilon_1\left(k_1(1-\alpha)\left(1-\frac{3}{2}k_1\right)\right.\\&\left.+\alpha k_2\left(1-\frac{3}{2}k_2\right)-\frac{3}{2}k_1k_2+\frac{1}{2}\right),\end{aligned}$$

$$\mu_0^p=\frac{\epsilon_3+\epsilon_4-z\epsilon_1}{2}\left((1-\alpha)k_1^2+\alpha k_2^2+k_1k_2\right)+(z-2)\left(\epsilon_4-\frac{3}{2}\epsilon_1\right)(1-(1-\alpha)k_1-\alpha k_2),$$

$$\mu_0^s=-\epsilon_2\frac{z}{2}, \tag{11}$$

and

$$\epsilon_1=\epsilon_{us}-\epsilon_{uu},\quad \epsilon_2=\epsilon_{us}-\epsilon_{ss},\quad \epsilon_3=\epsilon_{xx}-\epsilon_{uu},\quad \epsilon_4=\epsilon_{pp}-\epsilon_{uu}. \tag{12}$$

In polymer chemistry literature, the coefficients, χ, μ_0^p, μ_0^s, are referred as the Flory interaction parameter and the chemical potentials of pure polymer and solvent species respectively (Keener et al., 2011b; Flory, 1953). The factor 1/2 in the per-particle interaction energy in Eq. (10) is to correct for double counting. The corresponding contributions to chemical potentials are

$$\mu_p^I=k_BT_0\left(\chi\phi_s^2+\mu_p^0\right), \tag{13a}$$

$$\mu_s^I=k_BT_0\left(\chi\phi_p^2+\mu_s^0\right). \tag{13b}$$

In summary, the chemical potential for the polymer and solvent phase is

$$\frac{\mu_j}{k_BT}=M_i+z_i\Psi_e+\nu_i\frac{P}{k_BT},\quad j=p,s, \tag{14}$$

where $\Psi_e=\Phi_e/k_BT$, $M_p=1/k_BT(\mu_p^S+\mu_p^I)$ and $M_s=1/k_BT(\mu_s^S+\mu_s^I)-\sigma_I$. For the ion species, $\mu_j^I=0$, and we ignore its volume, ν_j, so that

$$\frac{\mu_j}{k_BT}=\ln\phi_j+1-\sigma_I+z_j\Psi_e,\quad j\geq 4, \tag{15}$$

Finally, since there is a free moving-edge to the gel, on one side of which (inside the gel) $\theta_p=\theta_p^-$, and on the other side of which (outside the gel) $\theta_p^+=0$, $\theta_s^+=1$, there are interface conditions,

$$\frac{1}{\nu_p}\mu_p^-\mathbf{n}=\frac{k_BT}{\nu_p}\left(M_p^-+z_p\Psi_e+\nu_p\frac{P}{k_BT}\right)\mathbf{n}=0, \tag{16}$$

for the polymer, and

$$\frac{1}{\nu_s}(\mu_s^+-\mu_s^-)\mathbf{n}=\frac{k_BT}{\nu_s}\left(M_s^+-M_s^--\sigma_I^++\sigma_I^--\nu_s\frac{P}{k_BT}\right)\mathbf{n}=0, \tag{17}$$

for the solvent. $P\equiv P^-$, $P^+=0$ and $\Psi_e^-\equiv\Psi_e$, $\Psi_e^+=0$. $\mathbf{n}$ is the normal to the free surface. The interface conditions are derived using the standard variational arguments to minimize the rate of work, which constitutes the viscous rate of energy dissipated within the polymer and the solvent, energy dissipation rate due to the drag between solvent and polymer and between solvent and ion species particles as well as the rate of work required against the chemical potential, μ_j. Readers are directed to Keener et al. (2011a, 2011b) and Sircar et al. (2013) to see the derivation details. Eliminating P from Eqs. (16) and (17) we find the single interface condition at equilibrium swelling conditions

$$\Sigma_{net}\mathbf{n}=0, \tag{18}$$

where Σ_{net} is the net swelling pressure,

$$\frac{\Sigma_{net}}{k_BT}=\frac{M_p^-}{\nu_p}-\frac{M_s^-}{\nu_s}+\frac{T_0}{T}\frac{\mu_s^0}{\nu_s}+\frac{z_p}{\nu_p}\Psi_e+\frac{\sigma_I^-}{\nu_s}-\frac{\sigma_I^+}{\nu_s}. \tag{19}$$

The first three terms in the right-hand side of the above equation correspond to the swelling via entropic contribution, the fourth term represents swelling pressure coming from the fact that the monomers may be charged, i.e., the Donnan equilibrium ($z_p\Psi_e$ is the corresponding Donnan potential) while the last two terms represent the osmotic swelling pressure coming from the difference between the concentrations of ions dissolved in the gel and those dissolved in the bath ($(\sigma_I^--\sigma_I^+)$ termed as the 'Net Osmolarity').

2.2. Ionized-species chemistry

Let the concentrations per total volume of the monomer species be denoted by $m=[\mathrm{M^{2-}}], y=[\mathrm{MH^-}], v=[\mathrm{MNa^-}], w=[\mathrm{MH_2}], x=[\mathrm{MNa_2}], q=[\mathrm{MHNa}]$, with the total monomer concentration

$$m_T=m+y+v+w+x+q, \tag{20}$$

The concentrations per solvent volume of the ion species are denoted as $n=[\mathrm{Na^+}], h=[\mathrm{H^+}]$, and $c_l=[\mathrm{Cl^-}]$. With concentrations expressed in units of moles per liter, the relationship between ion particle fractions ϕ_j and concentrations c_j is $\phi_j=\nu_sN_Ac_j$, where N_A is Avagadro's number.

To describe the chemical reactions, we use the law of mass action. Since all the monomer species are advected with the polymer velocity $\mathbf{v}_p$, the monomer species evolve according to

$$\frac{\partial j}{\partial t}+\nabla\cdot(\mathbf{v}_pj)=R_j^+-R_j^-,\quad j=y,v,w,x,q, \tag{21}$$

where R_j^+, R_j^- are the forward and backward rates for the monomer binding reactions in Eq. (1), respectively. The ChS monomer concentration, m, is obtained from Eq. (20).

Under the assumption of fast chemistry, we set the r.h.s. in Eq. (21) to zero, which reduces into the following set of equations for each of the monomer species

(a) $k_hmh\theta_s+(k_{-h_2}w+k_{-hn}q)\phi_s^2=k_{-h}y\phi_s^2+(k_{h_2}yh+k_{hn}yn)\theta_s$

(b) $(k_nmn+k_{n_2}vn)\theta_s=(k_{-n}v+k_{-n_2}x)\phi_s^2$

(c) $k_{h_2}yh\theta_s=k_{-h_2}w\phi_s^2$

$$(d)\quad k_{n_2} v n\theta_s = k_{-n_2} x\phi_s^2$$

$$(e)\quad k_{hn} y n\theta_s = k_{-hn} q\phi_s^2 \tag{22}$$

Since the unbinding (dissociation) reactions are ionization reactions that require two "units" of solvent, we take the unbinding reaction rates to be $k_{-C}\phi_s^2$, $C = h, n, h_2, n_2, hn$, and because ChS monomers carry a double negative charge, $2k_{i_2} = k_i, k_{-i_2} = 2k_{-i}$, $i = n, h$ and $4k_{hn} = k_h + k_n, k_{-hn} = k_{-h} + k_{-n}$. Simplifying Eq. (22),

$$y = \frac{\theta_s}{K_h\phi_s^2} mh, \quad v = \frac{\theta_s}{K_n\phi_s^2} mn, \quad w = \left(\frac{\theta_s}{2K_h\phi_s^2}\right)^2 mh^2,$$

$$x = \left(\frac{\theta_s}{2K_n\phi_s^2}\right)^2 mn^2, \; q = \left(\frac{\theta_s}{\sqrt{K_h K_{hn}}\phi_s^2}\right)^2 mhn, \tag{23}$$

where $K_h = k_{-h}/k_h$, $K_n = k_{-n}/k_n$, $K_{h_2} = 4K_h$, $K_{n_2} = 4K_n$ and $K_{hn} = 4(k_{-h} + k_{-n})/(k_h + k_n)$.

Similarly, under the assumption of fast diffusion and chemistry, the law of mass action for the ion species (n, h, c_l) reduces into

$$C = C_b e^{-z_C \Psi_e} \tag{24}$$

with $C = h, n, c_l$, $z_n = z_h = 1$ and $z_{c_l} = -1$ and the subscript 'b' denotes the corresponding bath concentrations (Sircar et al., 2013). The electrostatic potential, Ψ_e, is determined by the electroneutrality constraint inside the gel, namely,

$$(n + h - c_l)\theta_s + z_p m_T = 0, \tag{25}$$

where z_p is the average charge per monomer. This charge depends on the residual charge of the unbound and the bound ChS monomers,

$$z_p m_T = -(2m + y + v). \tag{26}$$

Both the electrostatic potential and polymer particle fraction are assumed to be zero outside the gel. Electroneutrality in the bath requires that

$$n_b + h_b - c_{lb} = 0. \tag{27}$$

Finally, the 'Net-Osmolarity' in the gel, *Osm*, is

$$Osm = (n + h + c_l) - (n_b + h_b + c_{l_b}) = (n_b + h_b)(e^{-\Psi_e} + e^{\Psi_e} - 2), \tag{28}$$

which measure the excess moles of solute (inside the gel) per liter of solvent.

3. Experimental setup

Experimental validation of the model is performed by running a subset of experiments in tandem with the proposed computational experiments described below. Ionic gels are formed by co-polymerizing methacrylated chondroitin sulfate (containing approximately 16 methacrylates per molecule) and poly(ethylene glycol) dimethacrylate in deionized water with a photoinitiator and 365 nm light (Villanueva et al., 2010). Monomers are synthesized and characterized by ^{1}HNMR in the Bryant laboratory following well-established protocols (Bryant et al., 2004). Gels of varying cross-link density are achieved by changing the total monomer concentration in solution prior to polymerization (e.g., 10 wt%, 20 wt%, and 30 wt% Nicodemus et al., 2011). In our experience, the monomers are fully incorporated into the gel with no detectable soluble fraction. These gels are then allowed to reach equilibrium in deionized water (e.g., 24 h) and then placed into appropriate solution (pH, salt, etc.) to reach a new equilibrium.

To quantify the local configuration of the gels, the counter-ion concentrations and the osmolarity inside these gels, the following in-vitro experiments were performed and the results were utilized to validate the outcome of numerical simulations: (i) Vary the particle fraction of PEG:ChS in a salt-free, neutral bath ($H_b = 10^{-7}$ M), where α, the particle fraction of ChS, is: 0.1, 0.2, 0.3, 0.4, 0.5 and 1. This experiment is performed to determine the role of fixed charges. Since the ChS monomer volume and the density are constant, increasing the particle fraction of ChS directly corresponds to increasing its weight fraction. (ii) Vary the bath concentration of the monovalent salt within a range of concentrations, 0.1–1 M, and (iii) repeat experiments (i) and (ii) in a salt-free bath and variable pH for neutral hydrogels (i.e., $\alpha = 0$) as well as for ionic gels (i.e., $\alpha > 0$). The pH is varied in the range 3–8 to ensure that the model accurately captures the local variables (i.e. the volume fractions, θ_i, and the osmolarity), within the physiological range (Maroudas, 1979). Further, the above-mentioned three sets of experiments are repeated for gels with different cross-link fractions. Polymer volume fraction will be determined from equilibrium swollen volume and dry polymer volume measurements and compared to the numerically determined value. Based on our preliminary results (Fig. 2), we see excellent correlation between experimental and numerical results. The initial volume of the dry polymer, V_i, was determined from the initial mass, m_i, using a weighted density of PEG and ChS, as follows:

$$V_i = 0.1\left(\frac{m_i \cdot \%PEG}{\rho_{PEG}} + \frac{m_i \cdot \%ChS}{\rho_{ChS}}\right) \tag{29}$$

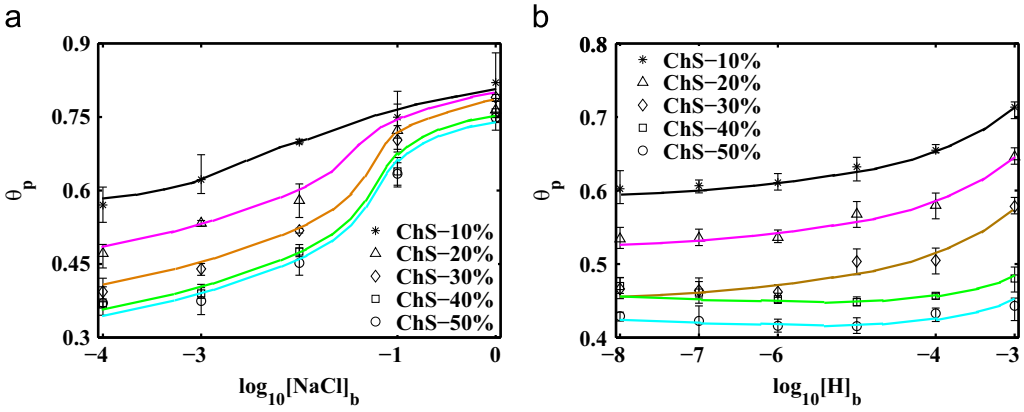

Fig. 2. Experimental data of equilibrium volume-fraction of the PEG-ChS gel vs. (a) different NaCl concentration in the bath (in mol/lt) and pH = 7.0, and (b) different pH and zero salt concentration. The gel sample is 10 wt% in solvent. The cross-link fraction of the PEG/ChS polymer pairs is 0.25/0.25, respectively. Notice the closeness of fit between the model output (i.e., solid lines) and the experimental data points.

The mass of the gel at equilibrium was measured and used to determine the swollen volume, $V_{swollen}$. It was assumed that all polymer was incorporated in the gel, which was confirmed for chondroitin sulfate, and therefore a change in mass was solely due to the change in the water content. Hence, for polymers with a 10 wt% dry weight in solvent,

$$V_{swollen} = 0.1\left(\frac{m_i \cdot \%PEG}{\rho_{PEG}} + \frac{m_i \cdot \%ChS}{\rho_{ChS}}\right) + \frac{m_{swollen} - 0.1 m_i}{\rho_{solvent}} \tag{30}$$

The initial mass, m_i, was the mass of the gel immediately following polymerization and before being placed in a solvent. The swollen mass, $m_{swollen}$, is the mass of the gel at equilibrium. The volume fraction of the polymer was calculated as the volume of the dry polymer (i.e. before swelling) divided by the volume of the swollen gel, $V_i/V_{swollen}$. The kinetic chains associated with methacrylate group (-MA) represents less than one percent of the total gel volume and therefore are not considered in the volume calculations.

4. Parameter estimation

The experimental data, collected from the list of experiments described in Section 3, are used to calibrate the model for the gel volume-fraction at equilibrium. Fig. 2 presents the sample averaged equilibrium data-points at different salt concentrations in a neutral pH sample (Fig. 2a) as well as in a salt-free, variable pH solution (Fig. 2b). The equilibrium values were noted at time $t=24$ h. Each point represents the average of four samples. The values are noted in identical conditions with the upper and the lower limits in the error bar representing maximum and the minimum variation from the average, respectively.

The values of the parameters used in our numerical calculations are listed in Table 1. The constants in the model are the monomer volumes, ν_1, ν_2, the coordination number of the PEG-ChS polymer lattice, z, and the nearest neighbor interaction energies, ϵ_i, assumed identically equal for both types of polymer (Eq. (12))). The undetermined constants are the binding affinities of the various cations with the gel, K_h, K_n (introduced in Eq. (23)).

The monomer volumes are found from the density and the molecular weight information ($\nu_i = M_i/(\rho_i * N_A)$). The cross-linked PEG-ChS matrix has a 3-D configuration, which suggests that we choose the coordination number, $z=6$, which mimicks a 3-D cubic lattice (Nicodemus et al., 2011). The standard free energies, $k_B T_0 \mu_p^0$ and $k_B T_0 \mu_s^0$ (Eq. (11)) and the interaction energies, ϵ_i (Eq. (12)) are found from the Hildebrand solubility data, δ_i (Barton, 1990). The standard free energy is the energy of all the interactions between the molecule and its neighbors in a pure state that have to be disrupted to remove the molecule from the pure state. The relation between the standard free energies and the solubility parameters (listed in Table 1) are

$$\begin{aligned} -k_B T_0 \mu_p^0(\alpha = 0) &= \nu_1 \delta_1^2 \\ -k_B T_0 \mu_p^0(\alpha = 1) &= \nu_2 \delta_2^2 \\ -k_B T_0 \mu_s^0 &= \nu_w \delta_w^2, \end{aligned} \tag{31}$$

where $\nu_w = 2 \times 10^{-23}$ cm^3 is the volume of 1 molecule of water at reference temperature, $T_0 = 298$ K. The negative sign in Eq. (31) indicates that $k_B T_0 \mu_p^0, k_B T_0 \mu_s^0 < 0$, since they are the interaction energies.

The molecular mass and the density of PEG were fixed at 4600 g/mol and 1.07 g/mL, while that of ChS were selected at 48,700 g/mol and 1.001 g/mL, respectively. These values give the monomer volumes of the PEG chains as $\nu_1 = 7.14 \times 10^{-21}$ cm^3, and that of ChS chains as $\nu_2 = 8.08 \times 10^{-20}$ cm^3. The density of the solvent, $\rho_{solvent}$, was assumed to be 1.00 g/ml (Milch, 1965). The Hildebrand solubility parameters for pure species (values given in Table 1) and the monomer volumes are used to calculate the interaction energies, ϵ_i ($i=1,\ldots,4$). Using the relations in Eq. (31), these values are fixed at $\epsilon_1 = 0.0, \epsilon_2 = 3.74, \epsilon_3 = 9.58, \epsilon_4 = -56.17$. The reference temperature of the experiments was fixed at $T_0 = 298$ K.

The undetermined parameters, namely the binding affinities, K_h, K_n (Eq. (23)) are computed by minimizing a nonlinear least-square difference function between the experimentally observed values of the equilibrium volume fraction, θ_p, and the corresponding model output (explained in Section 2), implemented via the MATLAB non-linear least-square minimization function **lsqnonlin**. These values are found as $\log_{10}(K_n) = -2.17$, $\log_{10}(K_h) = -3.65$. The closeness of fit between the model (highlighted by the solid lines) and the experimental data points is shown in Fig. 2.

5. Results and discussion

At equilibrium, we solve the system of equations given by the interface conditions, Eq. (18), monomer conservation, Eq. (20), ion motion, Eq. (24) and electroneutrality, Eq. (25). It is observed that the cross-link fraction of these gels is variable under identical experimental conditions. Therefore, we study the effect of cross-linking on the equilibrium configuration of the gels by selecting three different pairs of cross-link fractions for the PEG-ChS gels: CL_1: (0.25, 0.25), CL_2: (0.35, 0.5) and CL_3: (0.45, 0.75). In the next subsections we delineate the equilibrium state of the unconfined gels versus three different physiochemical stimuli, namely the charge density (Section 5.1), bath salt concentration (Section 5.2) and bath pH (Section 5.3).

5.1. Effects of changes in the gel composition

The first set of numerical experiments are designed to find the relation between the equilibrium configuration and the particle fraction of the charged component of the gel, α, of the gel. The experiments are repeated for gels with different cross-link fractions, (k_1, k_2). Fig. 3a,b,c present the equilibrium volume fraction, corresponding Donnan potential and the net-osmolarity vs. the particle fraction, α, respectively. It can be shown that the average charge per monomer (or the average ionization) increases in proportion to the particle fraction, α. The gel is dissolved in salt-free, neutral water ($[H]_b = 10^{-7}$ M). Any far field boundary effects are neglected in our numerical simulations, by assuming infinite

Table 1
Parameters common to all the numerical results. The reference temperature for the solubility parameters is fixed at $T_0 = 298$ K.

	PEG ($i=1$)	ChS ($i=2$)	Units	Source
Density (ρ_i)	1.07	1.001	g/mL	Bryant et al. (2004) and Milch (1965)
Molecular weight (M_i)	4600	48,700	g/mol	Bryant et al. (2005)
Repeat unit per chain (N_i)	102	86	–	Bryant et al. (2005)
Cross-link fraction (k_i)	0.25, 0.5, 0.75	0.25, 0.35, 0.45	–	Bryant and Anseth (2003)
Hildebrand solubility (δ_i)	17.39	5.19	MPa$^{1/2}$	Barton (1990)
Hildebrand solubility for water (δ_w)		48.07	MPa$^{1/2}$	Barton (1990)

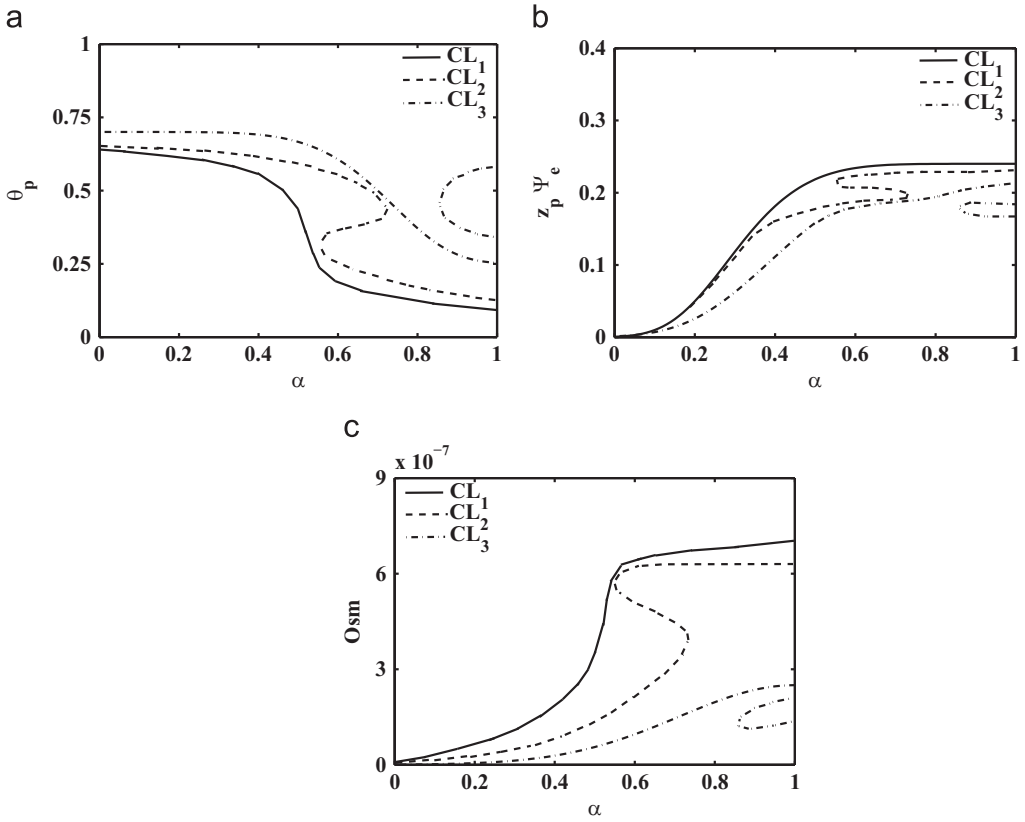

Fig. 3. (a) Equilibrium polymer volume-fraction, (b) Donnan potential, and (c) net-osmolarity in neutral salt-free, bath conditions vs. α, the particle fraction of chondrotin sulfate component for gel solutions with different cross-link fractions.

bath conditions. The negative charges on the gel causes water to dissociate into hydrogen (H^+) and hydronium (OH^-) ions. The free H^+ ions can bind with the monomers according to the binding reaction

$$M^{2-} + H^+ \underset{k_{-h}}{\overset{k_h}{\rightleftharpoons}} MH^-, \quad MH^- + H^+ \underset{k_{-h2}}{\overset{k_{h2}}{\rightleftharpoons}} MH_2 \tag{32}$$

Our numerical investigations reveal that there are qualitatively three different types of equilibrium swelling curves. If the cross-link fractions of the PEG/ChS polymer pairs is relatively low (e.g., the solid curve represented by the cross-link fraction pair, CL_1), there is a gradual swelling of the gel as the particle fraction, α, is increased. This transition is known as a second order/continuous volume transition. Otherwise, the gel can have there equilibrium states, depending on α, with hysteretic swelling-deswelling phase transition behavior which is either reversible (dashed curve, Fig. 3a) or irreversible (dash-dot curve). That is, in general at higher values of cross-link fractions there is a discontinuous (first order) swelling transition with increasing α or a discontinuous (first order) deswelling transition with decreasing α. An exception to this rule is seen for highly cross-linked gels when the gel deswells with increasing α (e.g., the disjoint branch of the dash-dot curve represented by the cross-link fraction pair, CL_3). The reason for this exception is explained below.

With our choice of parameters, the uncharged gel has a unique equilibrium (i.e. '$\theta_p(\alpha = 0)$' is unique). However, the appearance of three solutions for a range of α should not be a surprise. It results due to changes in the Donnan pressure which is a function of the binding chemistry of the gel. The swelling pressure that result make the total free energy (Eq. (2)) into a double-well potential for certain particle fraction values, α, although this free energy is a single-well potential for uncharged gels.

There is an inverse relation between the volume fraction, θ_p (Fig. 3a) and the Donnan potential, $z_p\Psi_e$ (Fig. 3b). That is, increasing $z_p\Psi_e$ closely correlates with decreasing θ_p. This is easily understood since the gel-swelling occurs due to increasing swelling pressure (Eq. (19)). The dominant contributions to the swelling pressure arise from those due to entropy, Donnan pressure and the osmotic pressure. At equilibrium these must be in balance. At low cross-link fractions and for long chain polymers, the entropic contribution to the swelling pressure is negligible (due to the factors '$1/N_1$' and '$1/N_2$', Eqs. (7a)–(7c)). For all parameter values examined in this study, the pressure contribution via Donnan potential dominates the pressure due to osmotic potential. In fact, osmotic pressure difference due to the dissolved ions, is about six orders of magnitude smaller than the corresponding pressure due to Donnan potential in the range of parameters considered (Fig. 3c). Hence, an increase in the Donnan potential positively impacts the swelling pressure and leads to gel swelling.

For higher cross-link fractions and higher particle fraction values, the gel experiences deswelling with increasing α (i.e., the disjoint branch of dash-dot curve, Fig. 3a). This could be explained as follows. For our selected range of parameters and at sufficiently high cross-link fraction and particle fraction values, the term '$k_2/2N_2\alpha(\phi_2^{-2/3} - 3)$' in the polymer entropy is negative (Eq. (7a)) and offsets the increasing contribution from the Donnan potential. The total swelling pressure decreases for these values of cross-link fraction and particle fraction, which leads to gel deswelling. Experiments corroborate that a highly cross-linked network provides a barrier against the Donnan potential and deswells at higher ionization levels (Muir et al., 1970; Khare and Peppas, 1995).

In summary, the physically relevant solutions generally swell as a function of increasing α. The physically relevant solutions are the largest and smallest ones, if there are three solutions, because the

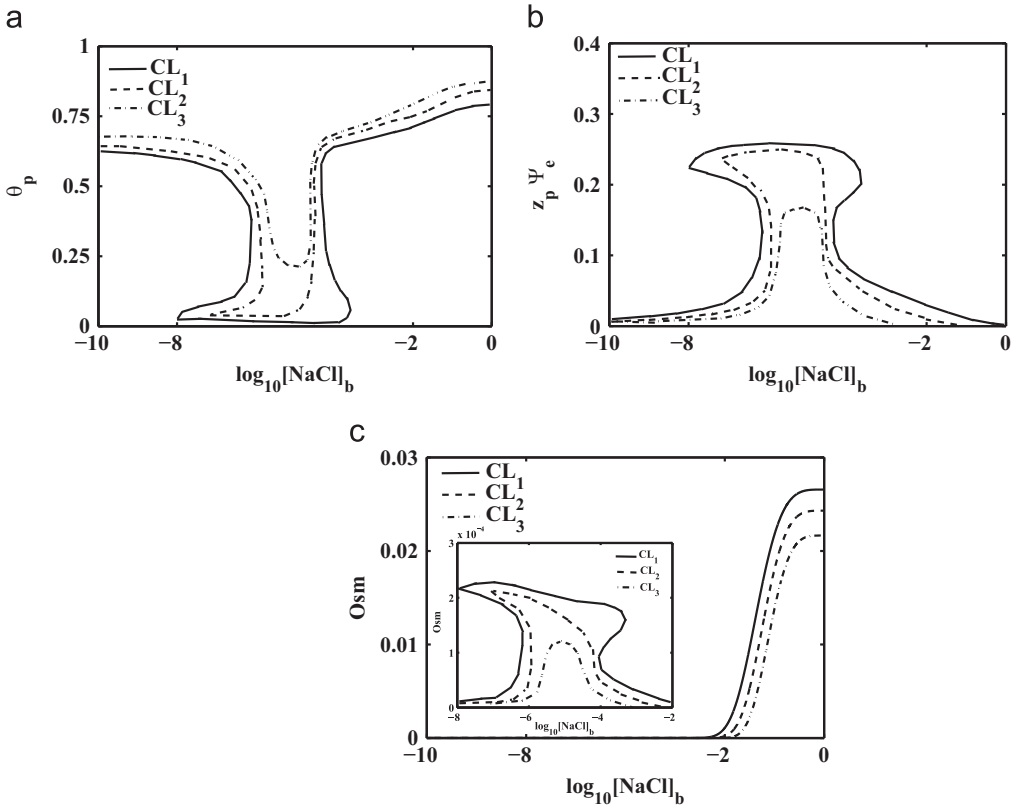

Fig. 4. (a) Equilibrium polymer volume-fraction, (b) Donnan potential, and (c) net-osmolarity, vs. NaCl-concentration (in mol/lt.) in the bath. Different curves represent samples a fixed ChS particle fraction, $\alpha = 0.1$, and variable cross-link fractions. Note the match in the equilibrium volume-fraction and the experimental data (Fig. 2a) in the range, $-4 \leq \log_{10}[\mathrm{NaCl}]_b \leq 0$.

intermediate solution is unstable. However, the gel deswells versus increasing α, at high cross-link fraction and certain range of particle fraction values. This exception highlights the impact of covalent cross-links which resist gel-swelling due to the effects of the Donnan potential and osmotic pressure of the dissolved counter-ions.

5.2. Effects of changes in the bath salt concentration

Next we numerically investigate the equilibrium solutions when the gel is immersed in an infinite bath with fixed hydrogen concentration ($H_b = 10^{-7}$ M) and containing a monovalent salt (i.e., a salt which furnishes monovalent cations when dissolved in water, e.g., Na^+). The simultaneous binding reactions of the negatively charged gel with two cations (i.e., H^+, Na^+) are listed in Eq. (1). Fig. 4a,b,c highlight the corresponding equilibrium volume fraction, Donnan potential and the net-osmolarity vs. the bath salt concentration, $[\mathrm{NaCl}]_b$, for gels with different cross-link fractions but a fixed ChS particle fraction, $\alpha = 0.1$, respectively. Usual features emerge at high concentrations ($[\mathrm{NaCl}]_b \geq 10^{-3}$ M) and low concentrations ($[\mathrm{NaCl}]_b \leq 10^{-8}$ M) of salt. At higher salt concentrations, the gel deswells and the deswelling is more prominent for specimen with greater cross-link fraction. This is readily understood since at higher salt concentrations, more dissolved Na^+ ions are furnished which can bind with the negatively charged gel. As a result, the primary ingredient of swelling pressure, i.e., the Donnan potential, is negligible (Fig. 4b). High cross-link density within the gel resists the swelling pressure which further enhances the deswelled state of the gel. At lower concentrations of salt, there any hardly any Na^+ (or H^+) ions readily available to bind with the gel. The Donnan potential is nearly constant and this feature leads to a fixed equilibrium state of the gel ($\theta_p \approx 0.65$).

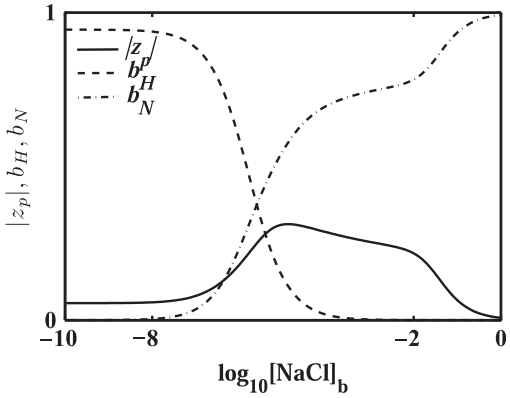

Fig. 5. Plots of average charge per monomer $|z_p|$ (solid curve), hydrogen binding fraction b_H (dashed curve) and sodium binding fraction b_N (dash-dot curve) vs. bath concentration of salt, $[\mathrm{NaCl}]_b$, for ChS particle fraction, $\alpha = 0.1$, and cross-link fractions, $k_1 = 0.35$, $k_2 = 0.5$.

For intermediate salt concentrations ($10^{-8} < [\mathrm{NaCl}]_b < 10^{-3}$ M), a new swelling-deswelling feature emerges, namely, there is a swelling, either gradual or through a phase transition, as the salt concentration in the bath increases. The explanation for these swelling feature is that there is a complicated interplay between ionization (which promotes swelling) and increases in bath concentration of salt which promote deswelling. This is illustrated in Fig. 5 where the total ionization, represented by the average charge per monomer $|z_p|$, hydrogen binding fraction $b_H = (y+w+q/2)/m_T = ([\mathrm{MH}^-]+[\mathrm{MH_2}]+[\mathrm{MHNa}]/2)/m_T$ and sodium binding fraction $b_N = (v+x+q/2)/m_T = ([\mathrm{MNa}^-]+[\mathrm{MNa_2}]+[\mathrm{MHNa}]/2)/m_T$ are

plotted vs. $[NaCl]_b$ for the specific case in which the cross-link fractions $k_1=0.45$ and $k_2=0.75$ (the curve represented by CL_3, see Fig. 4). In Fig. 5, we see that as $[NaCl]_b$ increases, there is an increase in sodium binding, and a decrease in hydrogen binding, with the net effect of an initial increase in the total ionization $|z_p|$, i.e., there is more unbinding of hydrogen than binding of sodium when the bath concentrations of the two ions are about the same ($Na^+ = H^+ \approx 10^{-7}$ M). The binding affinity of the sodium and hydrogen ions, with the gel, is $\log_{10} K_n = -2.17$ and $\log_{10} K_h = -3.65$, respectively. This implies that $K_n/K_h = 30.2$, or approximately every 1 Na^+ ion binding leads to unbinding of about 30 H^+ ions. This forces significant unbinding of hydrogen, leading to the observed net ionization.

As noted before, ionization promotes swelling and increased ion bath concentration promotes deswelling. For the selected values of material parameters, ionization swelling pressure dominates the ion bath concentration deswelling pressure. Thus, this ion exchange process explains the appearance of swelling regions in the swelling curves of Fig. 4. Additionally, we explored the equilibrium solutions vs. the bath salt concentrations for gels with variable ChS particle fractions but a fixed cross-link fraction and found that a swelled state was preferred at higher particle fraction values. This was due to a higher degree of ionization leading to a greater swelling.

5.3. Effects of changes in the bath pH

Finally, we explore the equilibrium state of an ionic gel immersed in a bath containing only hydrogen ions. The first set of numerical experiments involved predicting the equilibrium volume fraction of the charged gel with variable particle fractions (Fig. 6a). The cross-link fraction of the polymer matrix is fixed, $k_1 = k_2 = 0.25$. Hydrogen ions bind with the gel and the binding reactions are given in Eq. (32). The experiments reveal that qualitatively there are two types of equilibrium swelling curves, the reversible curves at lower particle fractions (e.g., solid and dashed curves), and the irreversible/disjoint curve at higher values of α (e.g., dash-dot curve), both of these curves highlight a first-order volume transition. Note that the pressure created by the Donnan potential is about an order of magnitude greater than potential induced osmotic pressure (comparing magnitude in Fig. 6b vs. Fig. 6c) as well as an order of magnitude greater than the pressure due to entropy. This implies that swelling is aided by the ionization which is induced by the Donnan potential. Since ionization is a positive function of the particle fraction of the charged gel, α, increasing this fraction leads to greater swelling (e.g., comparing magnitude of θ_p represented by the solid curve vs. dash-dot curve, Fig. 6a). Conversely, increasing the bath concentration of hydrogen leads to an increase in the dissolved cations which readily bind with the gel, thereby decreasing the ionization which leads to deswelling.

Another set of numerical simulations was carried to determine the equilibrium solutions of gels having a fixed ChS particle fraction but a variable cross-link fraction. It was found that gels progressively preferred a deswelled state in the order of increasing cross-link fraction values, consistent with our observations in Section 5.2. In summary, for the values of parameters examined, the gel swells predominantly due to effects of increasing Donnan potential and deswells due to the combination of increasing bath concentration of cations and increasing covalent cross-links within the polymer matrix.

6. Conclusions

In this paper, we have provided a multi-phase, multi-species model to quantify the swelling/de-swelling mechanism for

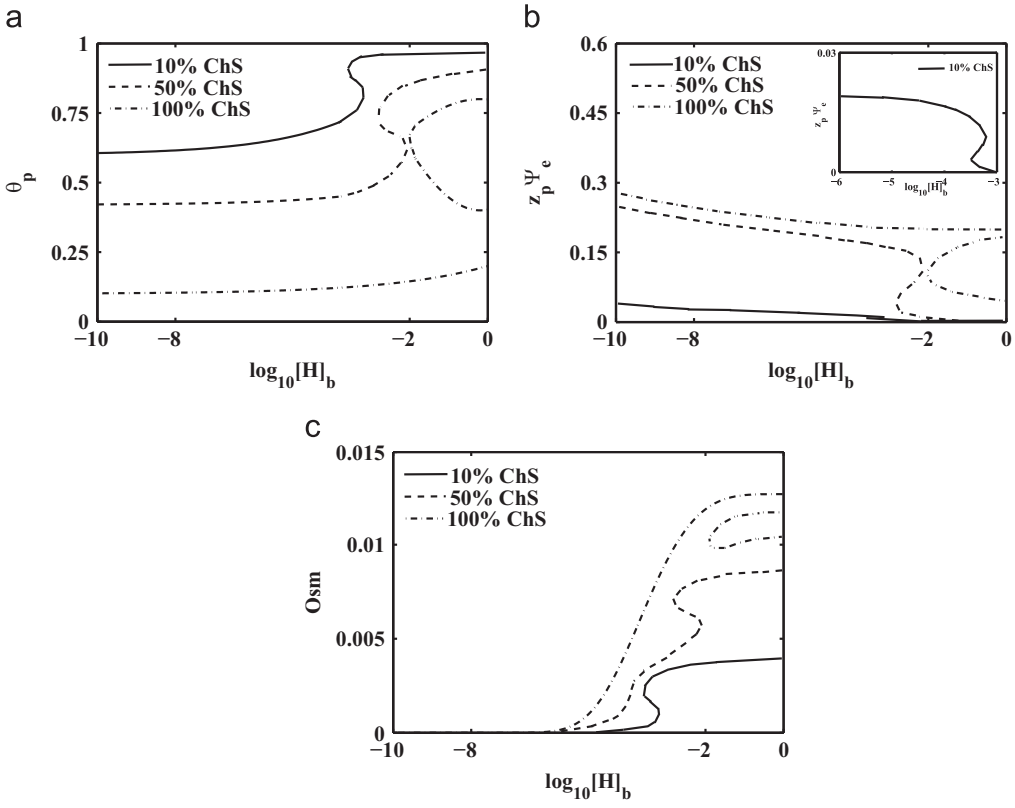

Fig. 6. (a) Equilibrium polymer volume-fraction, (b) Donnan potential, and (c) net-osmolarity vs. hydrogen bath concentration H_b, for a gel with fixed cross-link fraction $k_1 = k_2 = 0.25$ and variable composition of ChS. Note the match in the equilibrium volume-fraction and the experimental data (Fig. 2b) in the range, $-8 \leq \log_{10}[H]_b \leq -3$.

polylelectrolyte gels with covalent cross-links. Using this model we have examined the effects of the changes in the average charge per monomer (via variations in the chondrotin sulfate particle fractions), the bath concentration of monovalent solute (i.e., [NaCl]), the pH and the cross-link fraction of the gel on the equilibrium configuration. We conclude that, generally speaking, increasing the bath concentration of the ion species as well as the cross-link fraction of the gels per volume of total solution leads to deswelling while increasing the pH, the average charge per monomer leads to swelling, in agreement with experimental observations (Bryant and Anseth, 2003; Bryant et al., 2004, 2005). However, because of complex interactions between competing effects (e.g., pressure due to Donnan and osmotic potential which aids swelling and the elastic potential from covalent cross-links which helps de-swelling), the swelling/de-sweling mechanism is non-linear (or hysteretic) exhibiting either a first order (or discontinuous) transition or a second order (or continuous) transition in some situations. The full study of the kinetics of swelling of these gels under spatio-temporally varying mechanical loads will be the subject of a forthcoming article.

Acknowledgement

The in-vitro experiments were conducted via the financial support through the NSF CAREER Grant No. 0847390 of the Dr. Stephanie Bryant.

References

Armstrong, C.G., Mow, V.C., 1982. Variations in the intrinsic mechanical properties of human articular cartilage with age, degeneration, and water content. J. Bone Joint Surg. Am. 64, 88–94.
Barton A.F.M., 1990. Handbook of Polymer-Liquid Interaction Parameters and Solubility Parameters. CRC Press, Boca Raton, Florida.
Bryant, S.J., Anseth, K.S., 2003. Controlling the spatial distribution of ECM components in degradable PEG hydrogels for tissue engineering cartilage. J. Biomed. Mat. Res. 64 (1), 70–79.
Bryant, S.J., Davis-Arehart, K.A., Luo, N., Shoemaker, R.K., Aurther, J.A., Anseth, K.S., 2004. Synthesis and characterization of photopolymerized multifunctional hydrogels: water soluble poly(vinyl alcohol) and chondrotin sulfate macromers for chondrocyte encapsulation. Macromolecules 36 (7), 2556–2562.
Bryant, S.J., Arthur, J.A., Anseth, K.S., 2005. Incorporation of tissue-specific molecule alters chondrocyte metabolism and gene expression in photocrosslinked hydrogels. Acta Biomater. 1, 243–252.
Calderer, M.C., Chen, H., Micek, C., Mori, Y., 2013. A dynamic model of polyelectrolyte gels. SIAM J. Appl. Math. 73 (1), 104–133.
De, S.K., Aluru, N.R., Johnson, B., Crone, W.C., Beebe, D.J., Moore, J., 2002. Equilibrium swelling and kinetics of pH-responsive hydrogels: models, experiments, and simulations. J. Microelectromech. Syst. 11, 544555.
Dhanarajan, A.P., Misra, G.P., Siegel, R.A., 2002. Autonomous chemomechanical oscillations in a hydrogel/enzyme system driven by glucose. J. Phys. Chem. 106 (38), 8835–8838.
Doi M., 1996. Introduction to Polymer Physics. Oxford University Press; USA.
Doi, M., 2009. Gel dynamics. J. Phys. Soc. Jpn. 78 (5), 052001.
Doi, M., Edwards, S.F., 1986. Theory of Polymer Dynamics. Clarendon Press, Oxford, England.
Donnan, F.G., 1924. The theory of membrane equilibria. Chem. Rev. 1, 73–90.
Durning, C.J., Morman, K.N., 1993. Nonlinear swelling of polymer gels. J. Chem. Phys. 98, 4275–4293.
English, A.E., Mafe, S., Manzanares, J., Yu, X., Grosberg, A.Y., Tanaka, T., 1996. Equilibrium swelling properties of polyampholytic hydrogels. J. Chem. Phys. 104, 8713–8720.
Flory, P.J., 1953. Principles of Polymer Chemistry. Cornell University Press, Ithaca, NY.
Flory, P.J., 1976. Statistical thermodynamics of random networks. Proc. R. Soc. Lond. A. 351, 351–380.
Flory, P.J., Rehner, J., 1943a. Statistical mechanics of crosslinked polymer networks I. rubberlike elasticity. J. Chem. Phys. 11, 512.
Flory, P.J., Rehner, J., 1943b. Statistical mechanics of crosslinked polymer networks II. swelling. J. Chem. Phys. 11, 521.
Gu, W.Y., Lai, W.M., Mow, V.C., 1998. A mixture theory for charged-hydrated soft tissues containing multi-electrolytes: passive transport and swelling behaviors. Trans. ASME J. Biomech. Eng. 120, 169–180.
Health, United States, 2006 with chartbook on trends in the health of americans, DHHS Publication No. 2006-1232, Hyattsville, MD, 2006.
Hirotsu, S., 1991. Softening of bulk modulus and negative Poissons ratio near the volume phase transition of polymer gels. J. Chem. Phys. 94, 3949.
Hou, J.S., Holmes, M.H., Lai, W.M., Mow, V.C., 1989. Boundary Conditions at the cartilage-synovial fluid interface for joint lubrication and theoretical verifications. J. Biomech. Eng. 111 (1), 78–87.
Katchalsky, A., Michaeli, I., 1955. Polyelectrolyte gels in salt solutions. J. Polym. Sci. 15, 69–86.
Keener, J.P., Sircar, S., Fogelson, A., 2011a. Kinetics of swelling gels. SIAM J. Appl. Math. 71 (3), 854–875.
Keener, J.P., Sircar, S., Fogelson, A., 2011b. Influence of free energy on swelling kinetics of gels. Phy. Rev. E 83 (4), 041802.
Khare, A.R., Peppas, N.A., 1995. Swelling/deswelling of anionic copolymer gels. Biomaterials 16, 559–567.
Kokufuta, E., 2005. Polyelectrolyte gel transitions:? Experimental aspects of charge inhomogeneity in the swelling and segmental attractions in the shrinking. Langmuir 21 (22), 10004–10015.
Lai, W.M., Hou, J.S., Mow, V.C., 1991. A triphasic theory for the swelling and deformation behaviors of articular cartilage. J. Biomech. Eng. 113, 245–258.
Lanir, Y., 1996. Plausibility of structural constitutive equations for swelling tissues-implications of the c-n and s-e conditions. Trans. ASME J. Biomech. Eng. 118, 10–16.
Maroudas, A., 1968. Physicochemical properties of cartilage in the light of ion exchange theory. Biophys. J. 8, 57595.
Maroudas, A., 1979. Physicochemical properties of articular cartilage. Adult Articular Cartilage, 2nd ed., 215323.
Maroudas, A., Wachtel, E., Grushko, G., Katz, E.P., Weinberg, P., 1991. The effect of osmotic and mechanical pressures on water partitioning in articular cartilage. Biochim. Biophys. Acta 1073, 28594.
Maskawa, J., Takeuchi, T., Maki, K., Tsuijii, K., Tanaka, T., 1999. Theory and numerical calculation of pattern formation in shrinking gels. J. Chem. Phys. 110, 10993–10999.
Milch, R.A., 1965. Hydrated density of chondroitin sulfate preparations. Cell. Mol. Life Sci. 21 (10), 578–579.
Mow, V.C., Ratcliffe, A., 1997. Structure and function of articular cartilage and meniscus. Basic Ortho. Biomech. 2nd ed. 11377.
Mow, V.C., Ateshian, G.A., Spilker, R.L., 1993. Biomechanics of diarthrodial joints: a review of twenty years of progress. J. Biomech. Eng. 115, 46067.
Muir, H., Bullough, P., Maroudas, A., 1970. The distribution of collagen in human articular cartilage with some of its physiological implications. J. Bone Joint Surg. Br. 52, 55463.
Nicodemus, G.D., Skaalure, S.C., Bryant, S.J., 2011. Gel structure impacts pericellular and extracellular matrix deposition which subsequently alters metabolic activities in chondrocyte-laden peg hydrogels. Acta Biomater. 7 (2), 492–504.
Onuki, A., 1989. Theory of pattern formation in gels: surface folding in highly compressible elastic bodies. Phys. Rev. A 39, 5932–5948.
Sekimoto, K., Suematsu, N., Kawasaki, K., 1989. Spongelike domain structure in a two-dimensional model gel undergoing volume-phase transition. Phys. Rev. A 39, 4912–4914.
Setton, L.A., Zhu, W., Mow, V.C., 1993. The biphasic poroviscoelastic behavior of articular cartilage: role of the surface zone in governing the compressive behavior. J. Biomech. 26, 58192.
Sircar, S., Keener, J.P., Fogelson, A.L., 2013. The effect of divalent vs. monovalent ions on the swelling of Mucin-like polyelectrolyte gels: governing equations and equilibrium analysis. J. Chem. Phys. 138, 014901.
Tanaka, T., Filmore, D.J., 1979. Kinetics of swelling gels. J. Chem. Phys. 70, 1214–1218.
Tanaka, T., Filmore, D., Sun, S.T., Nishio, I., Swislow, G., Saha, A., 1980. Phase transition in ionic gels. Phys. Rev. Lett. 45 (20), 1636.
Villanueva, I., Gladem, S.K., Kessler, J., Bryant, S.J., 2010. Dynamic loading stimulates chondrocytes biosynthesis when encapsulated in charged hydrogels prepared from poly(ethylene glycol) and chondroitin sulfate. Mat. Biol. 29, 51–62.
Wang, C., Li, Y., Hu, Z., 1997. Swelling kinetics of polymer gels. Macromolecules 30, 4727–4732.
Wolgemuth, C., Mogilner, A., Oster, G., 2004. The hydration dynamics of polyelectrolyte gels with applications to cell motility and drug delivery. Eur. Biophys. J. 33, 146–158.
Yamaue, T., Taniguchi, T., Doi, M., 2000. Shrinking process of gels by stress-diffusion coupled dynamics. Prog. Theor. Phys. Supp. 138, 416–417.
Zribi, O.V., Kyung, H., Golestanian, R., Liverpool, T.B., Wong, G.C.L., 2006. Condensation of DNA-actin polyelectrolyte mixtures driven by ions of different valences. Phys. Rev. E 73, 031911.